Machine Learning-Based Assessment of the Impact of the Manufacturing Process on Battery Electrode Heterogeneity

Marc Duquesnoy, I. Boyano, L. Ganborena, P. Cereijo, E. Ayerbe, Alejandro Franco

Manufacturing Process on Battery Electrode Heterogeneity

Marc Duquesnoy[a,b,c], Iker Boyano[d], Larraitz Ganborena[d], Pablo Cereijo[d], Elixabete Ayerbe[c,d] and Alejandro A. Franco[a,b,c,e,*]

[a]*Laboratoire de Réactivité et Chimie des Solides (LRCS), UMR CNRS 7314, Université de Picardie Jules Verne, Hub de l'Energie, 15, rue Baudelocque, 80039 Amiens Cedex, France.*
[b]*Reseau sur le Stockage Electrochimique de l'Energie (RS2E), FR CNRS 3459, Hub de l'Energie, 15, rue Baudelocque, 80039 Amiens Cedex, France.*
[c]*ALISTORE-European Research Institute, FR CNRS 3104, Hub de l'Energie, 15, rue Baudelocque, 80039 Amiens Cedex, France*
[d]*CIDETEC, Basque Research and Technology Alliance (BRTA), Pº Miramón 196, 20014 Donostia-San Sebastian, Spain.*
[e]*Institut Universitaire de France, 103 Boulevard Saint Michel, 75005 Paris, France.*

ARTICLE INFO

Keywords:
Machine Learning
Electrode Manufacturing
Battery
Heterogeneity
Data Analysis

Abstract

Electrode manufacturing process strongly impacts lithium-ion battery characteristics. The electrode slurry properties and the coating parameters are among the main factors influencing the electrode heterogeneity which impacts the battery cell performance and lifetime. However, the analysis of the impact of electrode manufacturing parameters on the electrode heterogeneity is difficult to be quantified and automatized due to the large number of parameters that can be adjusted in the process. In this work, a data-driven methodology was developed for automatic assessment of the impact of parameters such as the formulation and liquid-to-solid ratio in the slurry, and the gap used for its coating on the current collector, on the electrodes heterogeneity. A dataset generated by experimental measurements was used for training and testing a Machine Learning (ML) classifier namely Gaussian Naives Bayes algorithm, for predicting if an electrode is homogeneous or heterogeneous depending on the manufacturing parameters. Lastly, through a 2D representation, the impact of the manufacturing parameters on the electrode heterogeneity was assessed in detail, paving the way towards a powerful tool for the optimization of next generation of battery electrodes.

Introduction

Lithium-ion batteries (LIBs) are under the spotlight in industrial applications, especially for the development of new portable devices and electric vehicles. LIBs are also intended to play a crucial role in the energy transition, leading to researchers and companies in sea- rch of improvement of the cell performance and durability while decreasing production cost. Certain areas of battery production have to be revisited to target low costs that are currently still too high for LIBs [1, 2]. For instance, NMP solvent is used while preparing the cathode electrode slurry that later is casted on a current collector, and adds significant cost in the electrode manufacturing process [3]. That is why deeper analysis in understanding the effect of manufacturing parameters on electrode properties is an utmost in order to accelerate the optimization of electrodes manufacturing.

For such optimization, the study of the slurry formulation is crucial since the stability and homogeneity of the electrode slurry affects the final electrode properties [4]. Previous studies have shown the importance of fabricating homogeneous electrodes whereas heterogeneous electrodes have lower transport properties (ionic and electronic), limiting cell performance and eventually inducing heterogeneous aging [5, 6]. The latter aspects directly reduce the effective energy and power densities, and compromise cell safety and lifetime [7]. Indeed, this implies an incomplete use of the active material within the electrode. For instance, Ouvard *et al.* characterized the heterogeneous behavior of electrodes through differences in distributions of $LiFePO_4$ proportions and stressed about the necessity to investigate the impact of manufacturing parameters on the the heterogeneous behavior of the electrodes [8].

Nevertheless, trial and error approaches have already demonstrated that LIBs performance is strongly correlated to electrode manufacturing conditions [9, 10, 11], more precisely through the slurry formulation and the calendering process [12]. That is why, such parameters are in the balance to reach an optimal configuration of the manufacturing process and to target desired performances [13], where a possible strategy is to deal with experimental measurements and analyzing their impact by data analysis methodology, in complement to computational physical-based simulations [14]. In that sense, the investigation of the electrode coating step will allow to better mitigate electrode heterogeneity [15].

Nowadays, Machine Learning (ML) approaches are becoming more popular in materials science [16] and in battery research, such as for performance predictions [17], Remaining Useful Lifetime (RUL) estimation [18], online estimation [19] or computational cost reductions [20]. Overall, ML algorithms are well-known for being very powerful at treating different types of data and at dealing with Big Data. Recently, various works focused on the application of such algorithms within the scope of battery manufacturing process, through supervised and unsupervised ML methods (such as random forest [21] and neural networks [22]) where the assessment of manufacturing parameters can be eased, accel-

*Corresponding author : alejandro.franco@u-picardie.fr
ORCID(s):

formance [10].

Recent publications have reported multi-objective data driven approaches to predict final battery properties by using different regression models [23]. Schnell *et al.* compared different regressions approaches such as linear models, ensemble learnings and artificial neural networks for predicting maximal capacity of battery cells as function of manufacturing data [24]. Weiss *et al.* focused on the application of usual ensemble lerning regression for the quality check of the speed of a wafer in the manufacturing process whereas Liu *et al.* applied ensemble learnings for classification purposes in the context of manufacturing feature importance and correlations [25]. Other data-driven approaches focused on the performance of cells manufacturing and concluded on the effect of the electrolyte mass on the cell maximum capacity [26]. Besides, other recent approaches focused more on the electrode formulation and calendering aspects, to embed experimental data and in silico electrode mesostructures features into a regression model in order to predict physical properties of calendered electrodes and in the meantime, bypass the calculation of properties based on physics-based models [27].

In this work, we propose an automatic approach combining unsupervised and supervised ML algorithms, supported by advanced statistical analysis, to predict LIBs electrodes properties in terms of mass loading and thickness, and systematically pinpoint NMC811 heterogeneous electrodes without any experimental labeling of the data. Such an approach is applied to unravel the effect of the slurry and coating parameters on such automatic heterogeneity definition, and provide a relevant and unique way to disclose such effect through 2D plots.

Experimental section

The heterogeneity study presented in this work was performed considering the cathode electrodes manufactured by casting a slurry onto an aluminium current collector. In particular, the slurry contained $LiNi_{0.8}Mn_{0.1}Co_{0.1}O_2$ (NMC811,Targray) as active material. This advanced cathodic material is characterized by having high voltaje and capacity. The slurry formulation also included conductive carbon (C65, Imerys) and poly-vinylidene fluoride (PVdF, Solef:5130, Solvay) as a binder in order to decrease the electrical resistivity and ensure the adherence and cohesion of the electrode, respectively.

2.1. Electrode preparation

For the analysis presented in this work, the electrode slurries were prepared by mixing the active material, conductive material and binder in a five liter planetary mixer (Inoue). First, the binder was dissolved in N-methyl pyrrolidone (NMP, Synthesis grade, Scharlab) by mechanical stirring to a final 5 *wt.%* concentration. Then, the binder solution and the conductive material were mixed in the planetary mixer. Afterwards, the active material was added to solvent was gradually added to the slurry during the mixing until reaching the final liqui-to-solid ratio.

Four different electrode formulations were prepared modifying the ratio of the three components of the electrode (*wt%* of active material, *wt%* of conductive additive, *wt%* of binder). Slurries with six different liquid-to-solid ratio values were prepared for each of the formulations. These six values are chosen among a set of eleven possible values ranging between 55 % and 73 %. Table 1 summarizes these values for active material (%AM), liquid-to-solid ratios (%LS) and gap.

The resulting slurries were casted on a 15 μm thickness Al foil (Hydro) by a knife coating system (Coatema). Electrodes with a coating length and width of 3 m and 0.210 m, respectively, and six different coating gaps, 50 μm, 75 μm, 100 μm, 200 μm, 300 μm and 400 μm, were prepared with each slurry. The wet films were dried in a three-zone oven system. Each zone is 1 m long and their temperatures are 100 $°C$, 110 $°C$ and 115 $°C$.

2.2. Electrode characterization

The homogeneity of the coating process was assessed by characterizing eighteen circular samples, distributed uniformly onto the electrode, measuring two parameters : thickness and mass loading. The electrodes were cut with a precision EL-cut device (EL-Cell) in disk format with 17.7 *mm* diameter. The circular samples were weighted using a precision balance (LAG 124i, VWR) and their thickness was measured with a precision micrometer (IP65, Mitutoyo).

Table 1
Different values of manufacturing parameters used to prepare the electrodes.

Parameter	Values
Active material [%]	{92.7, 94, 95, 96}
Liquid-to-solid [%]	{55, 58, 60, 63, 65, 67, 67.7, 68, 69, 71, 73}
Gap [μm]	{50, 75, 100, 200, 300, 400}

As a consequence, a set of 144 samples was obtained for the different electrode formulations. Those measurements are considered significant to represent a coated electrode by their mass loading and thickness values, with a the purpose to analyze the effect of manufacturing parameters on the final electrode heterogeneity.

Computational method

3.1. Heterogeneity definition

Mass loading and thickness are the two properties that were used to define the heterogeneity of coated electrodes (Figure 1). In particular, high variations of these two properties onto the electrode may realize a non-uniform mesostructure by

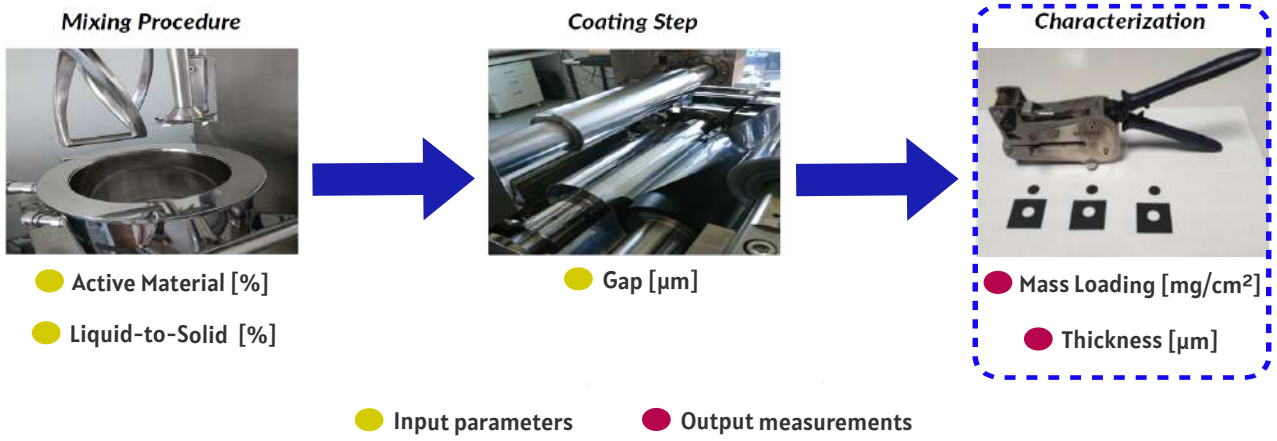

Figure 1: Workflow of the characterization along the steps of the manufacturing process considered in this work. The manufacturing parameters (yellow) and the output measurements (red) respectively correspond to influent parameters and trustable properties for heterogeneity definition.

modifying the slurry and coating manufacturing parameters. As a consequence, such physical interpretation is equivalent to calculate the relative standard deviation d_v (called *degree of variation* along the rest of the study) of the two properties, and analyze if such value is higher/lower than a threshold to conclude on the heterogeneity/homogeneity of the associated coated electrode. In that sense, the normalization of the standard deviation (*i.e.* σ) by the mean value (*i.e.* μ) of a sample like shown in Eq. 1, determines on what the heterogeneity of coated electrodes lies.

$$d_v = \frac{\sigma}{\mu} \qquad \text{(Eq. 1)}$$

The eighteen distributed circular electrode samples, detailed in the experimental section, are punched like shown in Figure 2. Nevertheless, instead of using all the eighteen samples to calculate the degree of variation in thickness and mass loading (*i.e.* $(d_v)_{\{thickness\}}$ and $(d_v)_{\{loading\}}$), the consideration of sub-samples of circular disks among all provide different degrees of variation calculations for one coating. Indeed, a grid of samples in a configuration of three rows and six columns, as Figure 2 shows, enables to define two possible measurements namely *Along* and *Perpendicular* configurations. As a consequence, the calculation enables three different degrees of variation according to each configuration. Therefore, the following analysis focuses on identifying meaningful degrees of variation to achieve the electrode heterogeneity definition, while changing the manufacturing parameters. Figure 3 shows the computational workflow adopted in this study, which is deeply described in the sections below. The Supporting Information summarizes the different nomenclatures used in this study.

3.1.1. Data compression

Firstly, a *Principal Component Analysis* (PCA) is applied to unravel interdependencies between the manufacturing parameters and the degrees of variation from coated electrodes, in combination with a segmentation method that classifies the 144 coated electrodes as heterogeneous or homogeneous. Nowadays, PCA is widely used in scientific research [28, 29, 30] and in electrochemistry [31] to treat a huge amount of quantitative data for a better understanding of the relationships among variables and appear relevant for the selection of the best initial variables to characterize heterogeneities. The idea behind the PCA is to find a linear combination of the m initial variables to construct fewer k orthogonal directions (with k smaller than m) with maximum variance. Those resulting directions are called principal components and identify the most relevant initial variables to describe the raw data. In that sense, The latter data can be projected on the subspace built by the principal components which realize how such data are spread along the new components. Therefore, PCA appears meaningful to analyze raw data defined with many initial variables, into straightforward 2D or 3D plots where axes are the principal components (see Figure S1 in the Supporting Information).

The linear combination requests k vectors to shape the matrix of projection called W. Considering raw data being $\tilde{x}_i$ explained by m variables in the vector space $\mathbb{R}^m$ like $\tilde{x}_i = [x_1, x_2, x_3, ..., x_m]$, the matrix W is a $m \times k$ matrix which allows to obtain the projection in the k-dimensional subspace. As a consequence, the projection of $\tilde{x}_i$ called c_i, is matrix-wise speaking written as

$$\tilde{x}_i^T W = c_i \quad c_i \in \mathbb{R}^k \qquad \text{(Eq. 2)}$$

The search of k vectors (*i.e. principal factors*) is under the constraint of maximum variance, also called inertia (*i.e.* I).

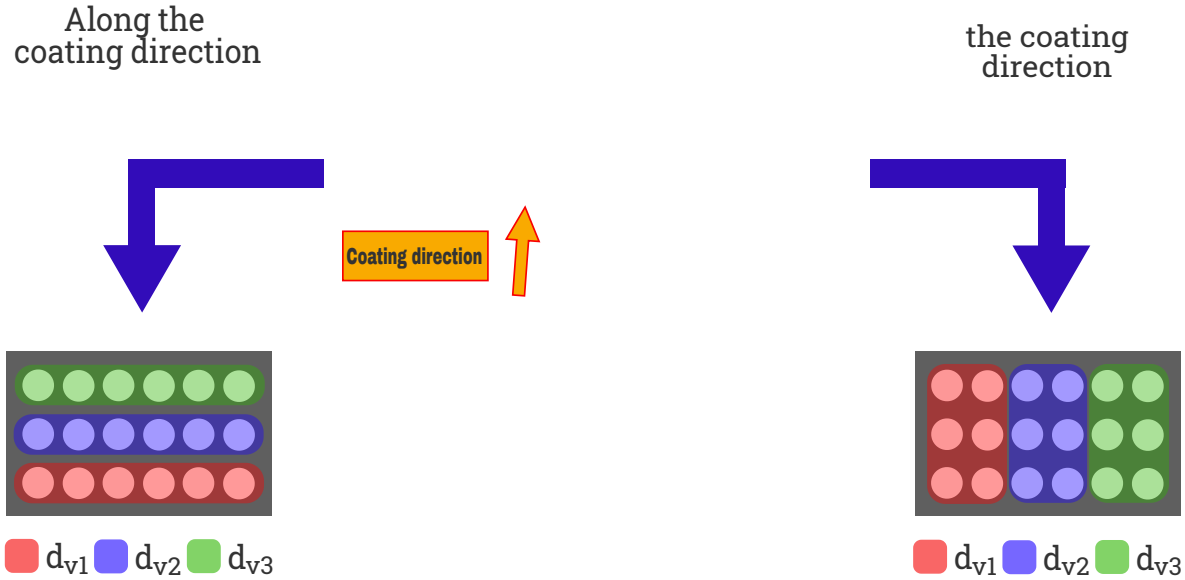

Figure 2: Scheme of the coating process and the distribution of the eighteen circular electrode punchs labelled in white, in terms of a grid configuration with three rows and six columns. Instead of calculating the degree of variation within the eighteen samples, two configurations are also taken into account for a calculation perpendicularly to the coating direction, and along it. $(d_{vi})_{i\leq 3}$ are different degrees of variation exactly calculated in the same conditions for both mass loading and thickness, each one with six circular disk samples per calculation. They have been color-coded separately for a better understanding of the approach. However, to avoid confusion in the following, the degrees of variation are noted as $d_{\{vi,perpendicular\}}$ and $d_{\{vi,along\}}$ for $i \in \{1,2,3\}$ for *Perpendicular* and *Along* configurations to avoid confusion.

That is why such research is equivalent to the following (P) problem :

$$(P) = \begin{cases} max \quad I(u) \\ u \in \mathbb{R}^N \\ ||u|| = 1 \end{cases} \qquad \text{(Eq. 3)}$$

with I being the inertia along a vector u and $||.||$ the Euclidean norm in the current vector space.

In that sense, solving (P) is equivalent to focus on the variance-covariance matrix $\Sigma = [\sigma_{ij}]_{i,j\leq m}$ due to the linear definition of the inertia in $\mathbb{R}^m$ (Eq. 5). Indeed, the latter matrix admits a singular values decomposition (*SVD*) and can be deconvoluted by m eigenvalues associated to m eigenvectors [32] as it follows :

$$\Sigma w_i = \lambda_i w_i \quad \lambda_i \in Spec(\Sigma) \qquad \text{(Eq. 4)}$$

From linear algebra, the inertia is equivalent to find the sum of eigenvalues [28] as

$$\begin{aligned} I &= \sum_{i\leq N} \frac{1}{N} \times d^2(\tilde{x}_i, g) \\ &= \sum_{i\leq m} \sigma_i^2 \\ &= Tr(\Sigma) \\ &= \sum_{i\leq m} \lambda_i \quad \lambda_i \in Spec(\Sigma) \end{aligned} \qquad \text{(Eq. 5)}$$

with $Tr(\Sigma)$ being the trace norm and $Spec(\Sigma)$ the set of eigenvalues.

As a consequence, obtaining most of the information (maximum variance) is equivalent to find the k highest eigenvalues, where the associated k eigenvectors represent the principal factors to form the matrix of projection. Similarly to Eq. 2, the complete projection of the initial dataset is assessed as it follows :

$$\begin{aligned} &[\tilde{x}_1, \tilde{x}_2, \tilde{x}_3, ..., \tilde{x}_N]^T \times [w_1, w_2, ..., w_k] = [c_1, c_2, ..., c_k] \\ &\iff XW = C \quad \forall \tilde{x}_i \in \mathbb{R}^m \end{aligned} \qquad \text{(Eq. 6)}$$

Figure 4 displays how close initial variables are with the principal components and then, how they contribute to their implementation. Indeed, a majority of variables appears meaningful for the PCA since the first five principal components reflect about 84 % of the initial information from the dataset. Such percentage seems relevant because the dimensionality reduction compresses the raw data and, in the meantime, the initial information. That is why the PCA gives a short subset of principal component where the variance is high.

As a consequence, a new PCA is performed without initial variables that contribute very little to the implementation of principal components. It does not affect the quality of the new subspace implementation since the projection of raw data figures out 94 % of the initial information within the

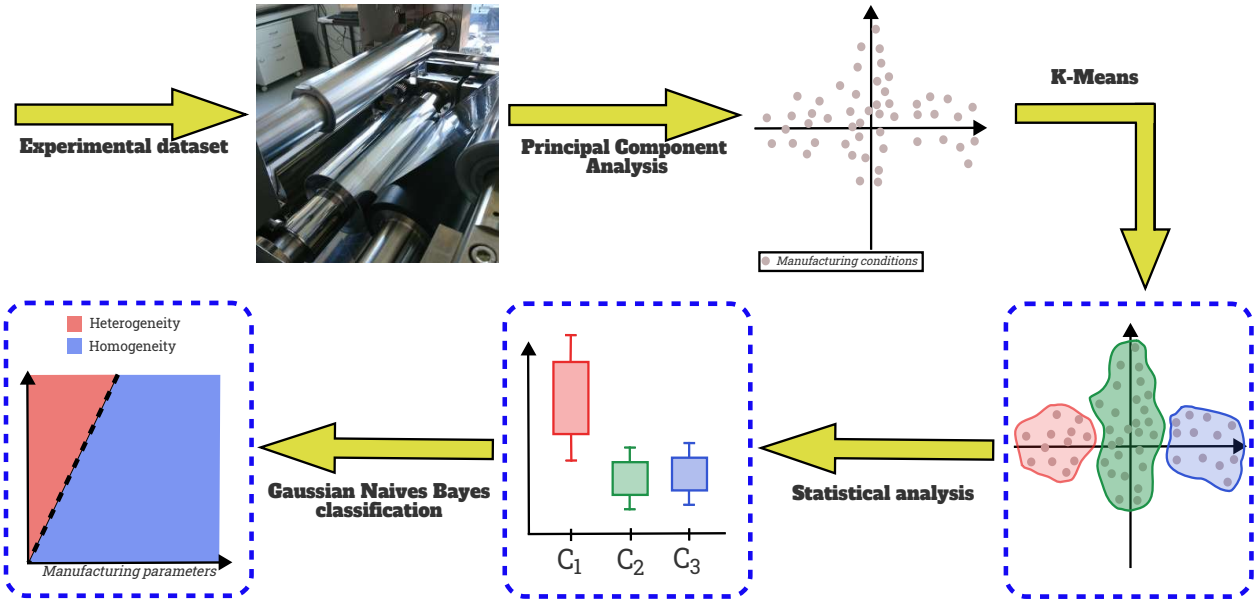

Figure 3: Computational workflow followed for the analysis of heterogeneous coated electrodes, from the experimental measurement till the design of the visualization tool.

first five principal components (see Figure S2 in the Supporting Information) and spreads correctly the manufacturing conditions along principal components for carrying out the subsequent heterogeneity definitions.

3.1.2. Segmentation methodology

A *K-Means* clustering is performed on the raw data from the variable subspace in order to obtain groups of manufacturing conditions [33]. This algorithm belongs to the unsupervised ML techniques and aims to separate raw data in different groups, also called *clusters*, with the same characteristics in terms of their initial variables, and without any ground truth category information. Indeed, the algorithm finds patterns of data to ensure the largest separation of the raw data by gathering them based on their feature similarities (see Figure S3 in the Supporting Information). Such methodology is relevant in the study since it gathers automatically the manufacturing conditions based on the data compression, and assesses a category to each manufacturing condition in the dataset for the further supervised learning classification into homogeneous or heterogeneous electrode, that is developed in this study.

The procedure is iterative, meaning that the raw data within the groups are optimized at each loop of the algorithm. These groups are characterized by k_c clusters by their centroid $(\mu_j)_{(j\leq k_c)}$. The later centroids represent the gravity centers of clusters and realize how far they are separated. As a consequence, seeking the best clusters is equivalent to minimizing the distance between raw data and centroids, which is the within-cluster sum of squares defined as follows

$$J = \sum_{i\leq N}\sum_{j\leq k_c} \omega_{i,j} \times ||\tilde{x}_i - \mu_j||^2 \quad (N, k_c) \in \mathbb{N}^2 \tag{Eq. 7}$$

where N represents the number of raw data points in the experimental dataset, and $(\omega_{i,j})$ a weight equals to 1 if the raw data $\tilde{x}_i$ belongs to the j^{st} cluster, else 0. The algorithm converges when J is not changing anymore, and provides the final centroids of each clusters with associated raw data.

Besides, the centroids are randomly chosen in order to initialize the algorithm. Then, the algorithm proceeds as follows :

- **i** Assign raw data to the nearest centroids μ_j to form clusters;
- **ii** Update the new centroids with associated raw data;
- **iii** Calculate the new value of the J metric;
- **iv** Iterate again from step i) to step iii) until reaching convergence.

The resulting groups are shown in Figure 5, with the raw data points color-coded in terms of the manufacturing conditions of the cluster to which they belong, with four (*i.e.* $k_c = 4$) groups in total. The k_c value can be chosen before launching the algorithm whereas inappropriate values can result into poor clustering performances. However in this study, the number of clusters was automatically chosen according to the *Elbow* method which identifies the most relevant number of clusters [34]. Indeed, the latter is tuned using

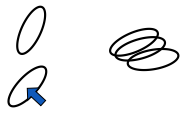

Figure 4: Projection of initial variables on the first principal plan. Arrows correspond to variables that are color-coded in black for manufacturing parameters, red for degrees of variation related to mass loading, green for degrees of variation related to thickness. The ellipses highlight the initial variables (*i.e.* arrows) that were removed to perform the second PCA. Lastly, the first and second principal components reflect 56 % and 25 % of the variance, respectively.

the *distortion* metric to compare performances for different values of k_c, and select the latter when such metric begins to appear stagnating most rapidly.

3.1.3. Heterogeneous conditions assessment

In order to compare the clusters, the non-parametric *Kruskal-Wallis* test is carried out to analyze statistically the distribution of $(d_v)_{\{loading\}}$ and $(d_v)_{\{thickness\}}$ between groups [35]. Such test appears meaningful when comparing more than two samples in order to conclude on the possible differences of medians between samples (*i.e.* from a statistical point of view, the samples are exactly the clusters), by assuming that residuals are not following a normal distribution. The significant result is assessed with the p-value of the associated statistical test. Such p-value can be interpreted as the probability to have the current data under the hypothesis of the test, where such value is compared to the smallest threshold which the hypothesis of the test is accepted [36]. Along the study, such p-value is written as p and compared to a threshold equals to 0.05 to conclude on the statistical test. The results are the following :

- A significant difference ($p \leq 0.05$) is found by comparing $(d_v)_{\{loading\}}$, and also $(d_v)_{\{thickness\}}$ between clusters. Besides, C_3 and C_4 are the clusters with different distributions meaning highest values, for thickness and mass loading variations respectively;
- C_1 and C_2 are the two remained clusters with the lowest values for both variables $(d_v)_{\{thickness\}}$ and $(d_v)_{\{loading\}}$. these clusters suggests lowest variations of mass loading and thickness properties. Therefore, the manufacturing conditions that C_1 and C_2 contain are associated to homogeneous coated electrodes;
- According to both configurations detailed in Figure 2, the same testing approach is made to compare the distribution of both $d_{\{vi,perpendicular\}}$ and $d_{\{vi,along\}}$ ($i \in \{1, 2, 3\}$) through clusters with highest values. No significant difference ($p > 0.05$) is found in the distribution comparison. That suggests that none part of the electrode has specific highest degrees of variation when a coated electrode has in average highest values of d_v. This allows concluding on the uniform heterogeneity along the total coated electrode (see Figures S4 and S5 in the Supporting Information).

Consequently to this statistical comparison and contrary to C_1 and C_2, the clusters C_3 and C_4 reflect larger variations in the electrode thickness and mass loading. The latter contain manufacturing conditions that produce heterogeneous coated electrodes in thickness and mass loading respectively. Such procedure provides an automatic assessment of heterogeneous electrodes from an experimental dataset, by analyzing specific manufacturing conditions aside from the rest. It also provides a labeling of the dataset with two binary output features representing two outputs for the ML algorithms detailed below, with value *0* meaning homogeneity and *1* heterogeneity. The binary variables are named as $\mathbf{1}_{\{loading\}}$ and $\mathbf{1}_{\{thickness\}}$ in the rest of the manuscript.

3.2. Modeling

The two binary variables are used as output to implement two classifiers, resulting from the definition of heterogeneities. Each model reflects the interdependencies between input parameters and heterogeneities by displaying trends along 2D plots. For the implementation of the models, the dataset is randomly splitted into training and testing data where the first one contains 80 % of the total standardized raw data and the latter the remaining 20 %. The training dataset is used to create and train models whereas the testing dataset evaluates the reliability of the developed model [37]. Indeed, the latter dataset contains experiments that are not seen by the model during the training, which is like if the model is tested versus experiments not carried out before.
It is important to point out unbalanced data while analyzing classes like Figure 6 shows where the majority of the data is categorized as homogeneous for both variables. This implies that the unbalanced dataset requires a resampling technique to adjust the classes distribution, which is in this study a random *oversampling* approach. Indeed, the latter adds synthetic samples to the under represented class [38]. Such a technique balances the classes distribution to improve the classifier performances when taking into account heterogeneous labels (*i.e.* unbalanced classes).

Figure 5: K-Means results from the clustering analysis represented on the first principal plan with groups C_1, C_2, C_3 and C_4 associated to the cluster centroid $(\mu_j)_{(j\leq 4)}$, color-coded in purple, blue, red and green respectively. The corresponding representation is straightforward interpretable for the spread of coated electrodes.

A *Gaussian Naives Bayes* (GNB) is the probabilistic technique applied, according to the data analysis presented above, for the supervised classification purpose. This technique has been already used in the domain of LIBs for regression problems such as RUL estimation [39], and it is used for binary classification purposes in the present study. Bayesian methods tend to be even more popular in the battery field, due to their intuitive definition and low requirement of parameters leading to low computational cost for learning [40, 41]. Indeed, a classification learning must predict the real class associated to given inputs, saying that Naives Bayes algorithm predicts the *a posteriori* probability $P(y|x_1, ..., x_m)$ to obtain each output class given all the inputs $(x_i)_{\{i\leq p\}}$ [42, 43]. More precisely, the definition of the model lies on the Bayes theorem where a *naive* hypothesis written in Eq. 9, reflects conditional independence of inputs for given class y.
Let's assume that heterogeneity and homogeneity classes are represented through the classification variable being $Y = y \in \{y_+, y_-\}$, a given observed dataset $\tilde{x} = (x_1, x_2, ..., x_m)$ $\forall (p, x_i) \in \mathbb{N} \times \mathbb{R}^N$. The Bayes theorem gives :

$$P(y|x_1, ..., x_m) = \frac{P(y) \times P(x_1, ..., x_m|y)}{P(x_1, ..., x_m)} \quad \text{(Eq. 8)}$$

$$P(x_1, ..., x_m|y) = \prod_{i=1}^{m} P(x_i|y) \quad \text{(Eq. 9)}$$

Meanwhile the algorithm considers the constant probability $P(x_1, ..., x_m)$ regarding the training dataset, and the output probability $P(y|x_1, ..., x_m)$ is approximated by the numerator. As a consequence, the following Bayes classifier $f(y)_x = \frac{P(y=y_+|x_1,...,x_m)}{P(y=y_-|x_1,...,x_m)}$ gives the rule consisting on finding y, the argument that maximizes the product of probability :

$$\begin{aligned} \hat{y} &= argmax_y(P(y) \times \prod_{i=1}^{m} P(x_i|y)) \\ &\Leftrightarrow f(y)_x \begin{cases} > 1 & \text{if } \hat{y} = y_+ \\ < 1 & \text{if } \hat{y} = y_- \end{cases} \end{aligned} \quad \text{(Eq. 10)}$$

In the case of this study, the probability distribution is assumed to be a multivariate Gaussian from $\mathbb{R}^m$ following the formula, which is simply the extension of the normal distribution in higher dimensions

$$P(x|y) = \frac{1}{\sqrt{(2\pi) \times det(\Sigma_y)}} * e^{-\frac{1}{2}(x_i-\mu_y)\Sigma_y^{-1}(x_i-\mu_y)^T} \quad \text{(Eq. 11)}$$

with parameters $\theta = (\mu_y, \Sigma_y)$, representing the mean vector and covariance matrix for data among one class y.

θ is estimated by the *Expectation-Maximisation* algorithm (EM) in order to compute the best fitting probability model

Figure 6: Unbalanced class distribution for cases (A) and (B) which correspond to $\mathbf{1}_{\{loading\}}$ and $\mathbf{1}_{\{thickness\}}$ respectively. It represents how each binary output is unbalanced with the number of electrodes in classes and their associated percentage of representativity for each binary classifier.

[44]. Indeed, the EM algorithm calculates the maximum for the likelihood $\ell(x, \mu_y, \Sigma_y) = \prod_{i=1}^{m} P(x_i|y))$ and get parameters of the distribution to conclude on the behavior of $f(y)_x$ [45]. The algorithm is iterative and used in the case of Gaussian mixture models (commonly called probabilistic models) [46].

In order to evaluate each model, the *Area Under Curve* (AUC) metric is used to analyze how testing data are well classified by the GNB models [47]. Besides, both models are used to avoid a bias induced in the metric value (given large variations) by operating many splits into training/testing datasets. However, they reflect an average AUC value of 0.91 and 0.84 with a very low variation, which is enough for the prediction capability of each classifier. The *AUC* metric is preferred for binary classification, more precisely because it measures how much a true positive observation (*i.e.* heterogeneous electrode) is predicted rather than a true negative observation (*i.e.* homogeneous electrode) without any consideration of a threshold [48]. In other words, the higher AUC is, the better the model predicts heterogeneity (homogeneity) for a heterogeneous (homogeneous) manufacturing condition.

Results and discussions

4.1. Prediction of heterogeneity

The built GNB models predict the *a posteriori* probability of the manufacturing heterogeneous/homogenous electrodes as a result of manufacturing parameters. Consequently, the 2D plots represent the evolution of the decision boundary of the model to produce heterogeneous electrodes at %AM compositions of 92.7 %, 94 %, 95 % and 96 %. Figures 7 and 8 capture, for mass loading and thickness respectively, the influence of input parameters (*i.e.* gap and %LS) on the evolution of heterogeneity. In this study, the predicting capability configuration are good enough according to AUC values for the prediction of the effect of manufacturing parameters.

According to the definition of the GNB for either $\mathbf{1}_{\{loading\}}$ or $\mathbf{1}_{\{thickness\}}$, when the probability is greater than 0.5, the electrode is classified as an heterogeneous one while it is classified as homogeneous for a value lower than 0.5.

4.2. Impact of manufacturing parameters

The classification reflects the relative weight of heterogeneity and homogeneity for manufacturing parameters ranges. The predicted patterns evolution in Figure 7 and 8 are different. In order to explain the reasons behind this trend, each output measurement is deeply analyzed for the search of interdependencies and the associated results are compared with different statistical tests (see Supporting Information). In this study, the distinction between the two different heterogeneities (illustrated in Figure 7 and 8) is useful for the interpretability of the effect of manufacturing parameters, since the coated electrodes adopt different types of mesostructures. Indeed, several rearrangements of active material particles inside the mesostructure may involve either a non-uniform, or uniform slurry in terms of mass loading, for the same thickness of the electrodes [49].

As a consequence, Figure 7 and 8 illustrate two different trends for the effect of the manufacturing parameters. They depend on the type of heterogeneity, such as the effect of the gap producing heterogeneous electrodes in thickness and mass loading at low values, whereas the effect of %AM is only noticeable on the heterogeneity in thickness.

4.2.1 Mass loading

According to Figure 7, the heterogeneity pattern appears in the left part of the 2D plots regardless the value of %AM. Indeed when decreasing the gap, the probability to be heterogeneous increases. As it can be also seen in Figure 7, there is no significant effect of %AM and %LS on the evolution of the heterogeneity pattern, symbolized with the curvature of the decision boundary that can be assimilated to a straight line. Indeed, while evaporating the solvent, the electrode is locally sensitive (*i.e.* unstable) to the particles distribution due to the compression at low gap leading to a non-uniform mesostructure, whereas the particles are uniformly distributed in a thick electrode at higher values of gap. Therefore, a statistical analysis is made, as a comparison, to check the trends found in Figure 7 (see Supporting Information for details). A significant relationship ($r^2 = -0.89$) is found between the gap and $(d_v)_{\{loading\}}$, whereas the dependence between %AM and $\mathbf{1}_{\{loading\}}$, and also between %LS and $\mathbf{1}_{\{loading\}}$ are not statistically significant ($p > 0.05$). Such results match with the empirical interpretation from Figure 7, allowed us concluding about the effect of the gap on the mass loading heterogeneity.

Figure 7: Classification results in terms of heterogeneity probability predictions for coated electrode mass loading, as a function of gap [μm], liquid-to-solid ratio [%], for different amounts of active material [%]. The 2D surface of probability predictions is interpolated in the parameters space, according to classification predictions based on manufacturing parameters combinations.

4.2.2 Thickness

The same approach is made to analyze the thickness heterogeneity. In this particular case, the outcomes of the implemented ML algorithms predict that with low %AM the probability of getting heterogeneous electrode is low, whereas at high %AM (*i.e.* 95 % and 96 %) heterogeneous electrodes can be expected for low gap values. Indeed, the heterogeneous pattern appears when %AM has a value between 94 % and 95 % In addition, for high %AM amount, the probability to obtain heterogeneous electrodes increases by decreasing the gap. There exists more mobility for particles at low values of binder content. As a consequence at low gap, such mobility provides a non-uniform distribution of particles giving a rough thin electrode after the evaporation of the solvent. In contrast, at high binder contents the cohesion between particles is favored leading to low probability of obtaining heterogeneous electrodes.
The same statistical approach discussed in the previous subsection is done leading to the same trends found in Figure 8 (see Tables S3 and S4 in the Supporting Information). Indeed, a significant relationship ($r^2 = -0.70$) is found between the gap and $(d_v)_{\{thickness\}}$ whereas the effect of slurry parameters on $\mathbf{1}_{\{thickness\}}$ is a combined effect (*i.e.* the effect of %LS depends on the values of %AM). The previous statistical analysis confirmed the trends found in Figure 8, and concluded the effect of slurry parameters (*i.e.* %AM and %LS) and the gap on such heterogeneity.

Conclusions

In this work a powerful Machine Learning-based approach to identify the most appropriate manufacturing conditions to enhance LIB electrode homogeneity is presented. Indeed, it was found relevant to analyze key parameters from the early steps of the manufacturing process, namely the amount of active material in the slurry, the liquid-to-solid ratio and the coating gap, with the purpose to automate the characterization of coated NMC811 electrodes as heterogeneous or homogeneous. Such methodology automatically proposed a definition of the heterogeneity based on the relative standard deviations calculation for punched disk samples. A *Principal Component Analysis* and *K-Means* clustering methods are combined to both pinpoint meaningful initial variables and classify the coated electrodes into groups of manufacturing conditions with the same characteristics in terms of in-

Figure 8: Classification results in terms of heterogeneity probability predictions for coated electrode thickness, as a function of gap [μm], liquid-to-solid ratio [%], for different amounts of active material [%]. The 2D surface of probability predictions is interpolated in the parameters space, according to classification predictions based on manufacturing parameters combinations.

put variables. Lastly, *Gaussian Naives Bayes* classifiers are tested to predict if the electrode associated to manufacturing parameters values is homogeneous or heterogeneous. Due to good performances, the resulting models gave the possibility to disclose graphically the relationship between manufacturing conditions and heterogeneity probabilities through straightforward 2D plots, where the validity was demonstrated with statistical tests. All these trends found are explained in terms of mass loading and thickness properties. As a consequence, this tool can be used for high throughput samples prediction as it allows assessing the data in a systematic and reliable way. It could also be transferred to electrodes made of other materials. Moreover, this tool avoids significant computational costs of physical-based computational simulations. Finally, our data-driven approach is essential to accelerate the optimization of LIBs manufacturing processes. Such methodology offers new opportunities to assess in a faster manner the impact of different manufacturing process steps on the final electrode properties, which is necessary to optimize LIBs.

Code and data availability

The codes and data are available for download from a Github repository upon publication of this paper :
ARTISTIC-ERC/electrode-heterogeneity

Supplementary data

Supporting Information in pdf format, giving an example of data compression and the graph of variance for the explanation of the PCA, an illustration of the K-Means algorithm, the graphical and statistical comparison of $d_{\{vi,perpendicular\}}$ and $d_{\{vi,along\}}$ for $i \in \{1, 2, 3\}$ in terms of mass loading and thickness, the statistical procedure applied for the effect of manufacturing parameters on heterogeneities, and lastly the complete nomenclature for acronyms used in this study.

Declaration of competing interest

The authors declare that they have no known competing financial interests or personal relationships that could have appeared to influence the work reported in this paper.

A.A.F. and M.D. acknowledge the European Union's Horizon 2020 research and innovation programme for the funding support through the European Research Council (grant agreement 772873, ARTISTIC project). M.D., E.A. and A.A.F. acknowledge the ALISTORE European Research Institute for funding support. A.A.F. acknowledges the Institut Universitaire de France for the support. We acknowledge Dr. Fernando Caro, postdoctoral researcher at LRCS, for the proofreading of the article and useful comments.

References

[1] M. Wentker, M. Greenwood, and J. Leker. A bottom-up approach to lithium-ion battery cost modeling with a focus on cathode active materials. *Energies*, 12:504, 2019.

[2] L. Slezak. Annual progress report 2009, office of freedom car and vehicle technologies. *U.S. Department of Energy, Washington*, 2009.

[3] D. L. Wood, J. Li, and C. Daniel. Prospects for reducing the processing cost of lithium ion batteries. *Journal of Power Sources*, 275:234–242, 2015.

[4] D. Liu, L-C Chen, T-J Lui, and C. Tiu. An effective mixing for lithium ion battery slurries. *Advances in Chemical Engineering and Sciences*, 4:515–528, 2014.

[5] A. Etiemble, N. Besnard, J. P. J. Adrien, Tran-Van, L. Gautier, B. Lestriez, and E. Maire. Quality control tool of electrode coating for lithium-ion batteries based on x-ray radiography. *Journal of Power Sources*, 298:285–291, 2015.

[6] H. Zheng, J. Li, X. Song, G. Liu, and V. S. Battaglia. A comprehensive understanding of electrode thickness effects on he electrochemical performances of li-ion battery cathodes. *Electrochemica Acta*, 71:258–265, 2012.

[7] W. A. Paxton, Z. Zhong, and T. Tsakalakos. Tracking inhomogeneity in high-capacity lithium iron phosphate batteries. *Journal of Power Sources*, 275:429–434, 2015.

[8] G. Ouvrard, M. Zerrouki, P. Soudan, B. Lestriez, C. Masquelier, M. Morcrette, S. Hamelet, S. Belin, A-M. Flank, and F. Baudelet. Heterogeneous behaviour of the lithium battery composite electrode lifepo4. *Journal of Power Sources*, 229:16–21, 2013.

[9] C. Meyer, M. Kosfeld, W. Haselrieder, and A. Kwade. Process modeling of the electrode calendering of lithium-ion batteries regarding variation of cathode active materials and mass loadings. *Journal of Energy Storage*, 18:371–379, 2018.

[10] R. P. Cunha, T. Lombardo, E. N. Primo, and A. A. Franco. Artificial intelligence investigation of nmc cathode manufacturing parameters interdependencies. *Batteries & Supercaps*, 3:60–67, 2020.

[11] W. Haselrieder, S. Ivanov, D. K. Kristen, H. Bockholt, and A. Kwade. Impact of the calendering process on the interfacial structure and the related electrochemical performance of secondary lithium-ion batteries. *Journal of The Electrochemical Society*, 165 (2):59–70, 2013.

[12] G. Lenze, H. Bockholt, C. Schilcher, L. Frobose, D. Jansen, U. Krewer, and A. Kwade. Impacts of variations in manufacturing parameters on performance of lithium-ion-batteries. *Journal of The Electrochemical Society*, 165 (2):314–322, 2018.

[13] N. Xue, W. Du, A. Gupta, W. Shyy, A-M. Sastry, and J. R. R. A. Martins. Optimization of a single lithium-ion battery cell with a gradient-based algorithm. *Journal of The Electrochemical Society*, 160 (8):1071–1078, 2013.

[14] B. Kenney, K. Darcovich, D. D. MacNeil, and I. J. Davidson. Modelling the impact of variations in electrode manufacturing on lithium-ion battery modules. *Journal of Power Sources*, 213:391–401, 2012.

[15] A. Ponrouch and M. R. Palacin. On the impact of the slurry mixing procedure in the electrochemical performance of composite electrodes for li-ion batteries: A case study for mesocarbon microbeads (mcmb) graphite and co_3o_4. *Journal of Power Sources*, 196:9682–9688, 2011.

using machine learning. *J Materiomics*, 3:159–177, 2017.

[17] D. Liu, J. Zhou, D. Pan, Y. Peng, and X. Peng. Lithium-ion battery remaining useful life estimation with an optimized relevance vector machine algorithm with incremental learning. *Measurement*, 63:143–151, 2015.

[18] S. Zhu, N. Zhao, and J. Sha. Predicting battery life with early cyclic data by machine learning. *Energy Storage*, 6:e98, 2019.

[19] A. Barre, B. Deguilhem, S. Grolleau, M. Gérard, F. Suard, and D. Riu. A review on lithium-ion battery ageing mechanisms and estimations for automotive applications. *Journal of Power Sources*, 241:680–689, 2013.

[20] C. Kavuri and S. L. Kokjohn. Exploring the potential of machine learning in reducing the computational time/expense and improving the reliability of engine optimization studies. *International Journal of Engine Research*, 21 (7):1251–1270, 2018.

[21] Y. Li, C. Zou, M. Berecibar, E. Nanini-Mauray, J. C.-W. Chan, P. vanden Bossche, J. Van Mierlo, and N. Omar. Random forest regression for online capacity estimation of lithium-ion batteries. *Applied Energy*, 232:197–210, 2018.

[22] J. Bao, V. Murugesan, C. J. Kamp, Y. Shao, L. Yan, and W. Wang. Machine learning coupled multi-scale modeling for redox flow batteries. *Advanced Theory and Simulation*, 1900167:1–13, 2019.

[23] A. Turetskyy, J. Wessel, C. Herrmann, and S. Thiede. Battery production design using multi-output machine learning models. *Energy Storage Materials*, 38:93–112, 2021.

[24] J. Schnell, C. Nentwich, F. Endres, A. Kollenda, F. Distel, T. Knoche, and G. Reinhart. Data mining in lithium-ion battery cell production. *Journal of Power Sources*, 413:360–366, 2019.

[25] K. Liu, X. Hu, H. Zhou, L. Tong, W. D. Widanage, and J. Marco. Feature analyses and modelling of lithium-ion batteries manufacturing based on random forest classification. *arXiv*, arXiv:2102.06029, 2021.

[26] T. Komas, R. Daub, M.Z. Karamat, S. Thiede, and Herrmann C. Data- and expert-driven analysis of cause-effect relationships in the production of lithium-ion batteries. *IEEE International Conference on Automation Science and Engineering*, pages 380–385, 2019.

[27] M. Duquesnoy, T. Lombardo, M. Chouchane, E. N. Primo, and A. A. Franco. Data-driven assessment of electrode calendering process by combining experimental results, in-silico mesostructures generation and machine learning. *Journal of Power Sources*, 480:229103, 2020.

[28] J. Shlens. A tutorial on principal component analysis. *arXiv*, abs/1404.1100, 2014.

[29] A. Giulliani. The application of principal component analysis to drug discovery and biomedical data. *Drug Discovery Today*, 22 (7):1069–1076, 2017.

[30] M. Ito, K.S Shimizu, and H. Honda. Searching for high-binding peptides to bile acid for inhibition of intestinal cholesterol absorption using principal component analysis. *Journal of Bioscience and Bioengineering*, 127 (3):336–371, 2019.

[31] C. Guellis, D. C. Valerio, G Bessegato, M. Boroski, J. C. Dragunski, and C. A. Lindino. Non-targeted method to detect honey adulteration: Combination of electrochemical and spectrophotometric responses with principal component analysis. *Journal of Food Composition and Analysis*, 89:103466, 2020.

[32] J. M. Lasgouttes. Variables quantitatives : Analyse en composantes principales. *https://who.rocq.inria.fr/Jean-Marc.Lasgouttes/anadonnees/cours-acp.pdf*, 2017.

[33] T. Kanungo, D. M. Mount, N. S. Netanyahu, C. D. Piatko, R. Silverman, and A. Y. Wu. An efficient k-means clustering algorithm : Analysis and implementation. *IEEE Transactions on Pattern Analysis and Machine Intelligence*, 24 (7):881–892, 2002.

[34] T. M. Kodinariya and P. Makwana. Review on determining number of clusters in k-means clustering. *International Journal of Advance Research in Computer Science and Management Studies*, 1 (6), 2013.

[35] P. E. McKnight and J. Najab. Kruskal-wallis test. *The Cosine Encyclopedia of Psychology*, 2010.

[36] J. D. Gibbons and J. W. Pratt. P-values: Interpretation and methodol-

[37] J. Brownlee. https://machinelearningmastery.com/train-test-split-for-evaluating-machine-learning-algorithms/. *Machine Learning Mystery*, 2020.
[38] T. Le, M. T. Vo, M. Y. Lee, and S. W. Baik. A hybrid approach using oversampling technique and cost-sensitive learning for bankruptcy prediction. *Hindawi*, 8460934, 2019.
[39] S. S.Y. Ng, Y. Xing, and K. L. Tsui. A naive bayes model for robust remaining useful life prediction of lithium-ion battery. *Applied Energy*, 118:114–123, 2014.
[40] C. Hu, G. Jain, C. Schmidt, C. Strief, and M. Sullivan. Online estimation of lithium-ion battery capacity using sparse bayesian learning. *Journal of Power Sources*, 289:105–113, 2015.
[41] B. Saha, K. Goebel, S. Poll, and J. Christophersen. Prognostics methods for battery health monitoring using a bayesian framework. *Journal of Power Sources*, 58 (2):291–296, 2009.
[42] S. Chen, G. I. Webb, Linyuan Liu, and X. Ma. A novel selective naïve bayes algorithm. *Knowledge-Based Systems*, 192:105361, 2020.
[43] H. Zhang. The optimality of naives bayes. *Proc. FLAIRS*, 2004.
[44] M. Collins. The naive bayes model, maximum-likelihood estimation, and the em algorithm.
[45] B. Panic, J. Klemenc, and M. Nagode. Improvised initialization of the em algorithm for mixture model parameter estimation. *Mathematics*, 8 (3):373, 2020.
[46] G. J. McLachlan and Krishnan T. The em algorithm and extensions. *Wiley Interscience*, 2nd edition, 2008.
[47] S. Wu and P. Flach. A scored auc metric for classifier evaluation and selection. *Workshop on Analysis in Machine Learning*, 2005.
[48] X. Zhang, X. Li, Y. Feng, and Z. Liu. The use of roc and auc in the validation of objective image fusion evaluation metrics. *Signal Processing*, 115:38–48, 2015.
[49] S. Yari, H. Hamed, J. D'Hen, M. K. Van Bael, F. U. Renner, A. Hardy, and M. Safari. Constructive versus destructive heterogeneity in porous electrodes of lithium-ion batteries. *Applied Energy Materials*, 3:11820–11829, 2020.

Declaration of interests

✔ The authors declare that they have no known competing financial interests or personal relationships that could have appeared to influence the work reported in this paper.

☐The authors declare the following financial interests/personal relationships which may be considered as potential competing interests:

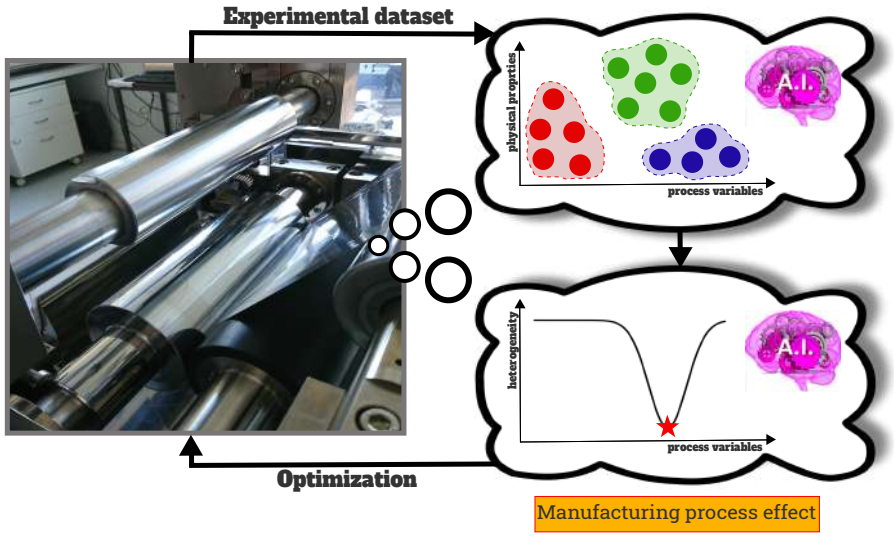
Experimental dataset
physical properties
process variables
A.I.
heterogeneity
process variables
A.I.
Optimization
Manufacturing process effect